THE JOURNAL OF PHYSICAL CHEMISTRY A
A JOURNAL OF THE AMERICAN CHEMICAL SOCIETY

pubs.acs.org/JPCA

Article

Experimental and Computational Description of the Interaction of H and H^- with U

Gabriel F. de Melo, Monica Vasiliu, Mary Marshall, Zhaoguo Zhu, Burak A. Tufekci, Sandra M. Ciborowski, Moritz Blankenhorn, Rachel M. Harris, Kit H. Bowen,* and David A. Dixon*

Cite This: *J. Phys. Chem. A* 2022, 126, 4432−4443

Read Online

ACCESS | Metrics & More | Article Recommendations | Supporting Information

ABSTRACT: The results of ab initio correlated molecular orbital theory electronic structure calculations for low-lying electronic states are presented for UH and UH^- and compared to photoelectron spectroscopy measurements. The calculations were performed at the CCSD(T)/CBS and multireference CASPT2 including spin−orbit effects by the state interacting approach levels. The ground states of UH and UH^- are predicted to be $^4I_{9/2}$ and $^5\Lambda_6$, respectively. The spectroscopic parameters T_e, r_e, ω_e, $\omega_e x_e$, and B_e were obtained, and potential energy curves were calculated for the low energy Ω states of UH. The calculated adiabatic electron affinity is 0.468 eV in excellent agreement with an experimental value of 0.462 ± 0.013 eV. The lowest vertical detachment energy was predicted to be 0.506 eV for the ground state, and the adiabatic ionization energy (IE) is predicted to be 6.116 eV. The bond dissociation energy (BDE) and heat of formation values of UH were obtained using the IE calculated at the Feller−Peterson−Dixon level. For UH, UH^-, and UH^+, the BDEs were predicted to be 225.5, 197.9, and 235.5 kJ/mol, respectively. The BDE for UH is predicted to be ∼20% lower in energy than that for ThH. The analysis of the natural bond orbitals shows a significant U^+H^- ionic component in the bond of UH.

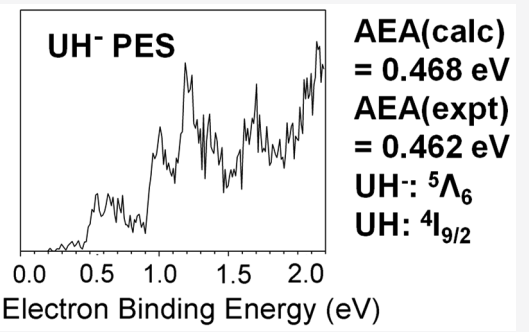

Downloaded via JOHNS HOPKINS UNIV on February 10, 2023 at 21:05:55 (UTC).
See https://pubs.acs.org/sharingguidelines for options on how to legitimately share published articles.

INTRODUCTION

Actinides and actinide-containing species are of special interest due to their unique chemical properties as well as their vital role in the field of nuclear energy.[1,2] Because most actinides are radioactive, expensive to produce, and difficult to handle, experimental studies alone present a challenge to understanding the basic properties of molecules containing actinides. This is exacerbated by the potential for many low-lying electronic states due to the presence of partially occupied 5f and/or 6d orbitals. Thus, a combination of experimental and theoretical approaches has become a useful approach for the study of the chemistry of heavy-element compounds. The uranium atom, one of the most studied actinides, has a $[Rn]5f^36d^17s^2$ electronic configuration with a ^5K_u excited state, only 620 cm^{-1} above the ^5L_u ground state; there are around 30 states below ∼2.0 eV in energy for U.[3] The chemistry of uranium is heavily dependent on its oxidation states with +4 and +6 being the most prevalent in natural compounds.[4] The potential presence of electrons in both the 5f and 6d valence orbitals plays a significant role in determining the nature of the bonding and reactivity of U. The potential for the existence of many low-lying excited states in uranium compounds with low oxidation states can require the use of multireference methods including relativistic corrections to identify their ground states and to match available spectroscopic values. So far, Tang et al.[5] have used slow-electron velocity-map imaging to obtain a value of 0.31497(9) for the electron affinity (EA) of U. Likewise, Bowen, Peterson, and co-workers[6] measured a value of 0.309 ± 0.025 eV for the EA(U) using negative ion photoelectron spectroscopy, in agreement with the above result. Based on composite coupled cluster theory with single and double excitations with perturbative triples (CCSD(T)) with all-electron four-component spin−orbit coupling, they calculated the EA of U to be 0.232 eV, corresponding to detachment from a 6d orbital on the U.

Several computational studies have been reported for uranium-containing diatomic molecules.[7−18] The electronic structure of uranium monohydride (UH) resembles those of UF and UCl, which can be considered ionic U^+X^-; the uranium cation is perturbed by a closed-shell anion ligand. Bross and Peterson[7] obtained a $^4I_{9/2}$ (U^+ ($5f^37s^2$) ground state for UF and UCl from high-level correlated molecular orbital theory calculations, in agreement with previous calculations on UF by Antonov and Heaven[8] using the CASPT2-SO approach. Dolg and co-workers[19,20] performed multireference (MRCI)

Received: May 5, 2022
Revised: June 14, 2022
Published: June 29, 2022

© 2022 American Chemical Society

https://doi.org/10.1021/acs.jpca.2c03115
J. Phys. Chem. A 2022, 126, 4432−4443

and relativistic calculations, at the all-electron DKH level and also with pseudopotentials (PP), on the low-lying states of UH with U $5f^3$ configurations. Their calculations predicted 16 states below ∼0.5 eV, also yielding a $^4I_{9/2}$ ground state. Andrews and co-workers[21,22] observed multiple uranium hydrides, UH_x (x = 1−4) and U_2H_x (x = 2,4), as products of laser-ablated U atoms reacting with gaseous H_2 and HF in solid Ar and Ne matrices. For UH, a vibrational band at 1423.6 cm^{-1} was assigned based on its density functional theory calculations for the quartet ground state. Recently, Armentrout and co-workers have carried out experimental kinetic reactions of an uranium atomic cation (U^+) with H_2, D_2, and HD via guided ion beam mass spectrometry determining a bond dissociation energy (BDE) of 2.48 ± 0.06 eV (U^+−H) for UH^+,[23] close to the one obtained experimentally for ThH^+ (2.45 ± 0.07 eV) by Cox et al.[24] Note that the experimental value for the BDE of ThH^+ does not agree with a high-level calculated value of 2.82 eV.[24,25] In the same work on UH,[23] they predicted a $^5\Phi$ ($\pi^2\sigma$) ground state with an excited ^{5}I ($\pi\delta\sigma$) state lying 0.006 eV (48 cm^{-1}) higher in energy at the CCSD(T) level of theory and a BDE equal to 2.43 eV at the CCSD(T)/CBS-cc-pw-CVnZDK3 level. After the inclusion of spin−orbit effects, the ^{5}I state was assigned as the ground state of UH^+. Using the CASPT2-RASSI approach with the relativistic DK2 Hamiltonian, these authors[23] obtained a spin−orbit correction of 0.779 eV (6283 cm^{-1}). We have previously used the methods described in the current work to obtain the thermodynamic properties of the $ThH^{0/-1/+1}$ diatomic molecules and interpret the PES spectra yielding very accurate results.[25] In that work, we also showed that the H/H^- ligand can provide insights into the atomic states of the actinide atom.

The goal of the current work is to investigate the electronic structures of UH and UH^- molecules using high-level computational electronic structure methods, with the intention of expanding our knowledge of the bonding and energetics of the uranium atom with different ligands in the gas phase. The photoelectron spectrum (PES) of UH^- is reported together with CCSD(T)/CBS and CASPT2 calculations including spin−orbit coupling using the state interacting approach. The energies of the low-lying excited electronic states and their rovibrational constants were calculated, as well as vertical detachment energies (VDE) from the anion, the adiabatic electron affinity (AEA), and the BDEs.

EXPERIMENTAL AND COMPUTATIONAL METHODS

Experimental Section. The UH^- and UD^- anions were produced and analyzed using a house-built anion photoelectron spectrometer, which has been described in detail previously.[26] The apparatus consists of an ion source, a time-of-flight mass spectrometer, a Nd:YAG photodetachment laser, and a magnetic bottle energy analyzer. The uranium hydride anions were generated in a laser vaporization ion source. A rotating, translating uranium rod was ablated using the second harmonic of a Nd:YAG laser (532 nm, 2.33 eV), while 20 PSI of UHP H_2 gas expanded over the U rod. After pulsing H_2 gas over the rod for a minute, the gas flow was shut off, and the experiments were conducting using no backing gas. In order to generate UD^- anions, the experiment was repeated with 15 PSI of D_2 expanded over the U rod. The backing gas was shut off because only diatomic UH^-/UD^-, the focus of the current work, were observed with no backing gas. Larger clusters like $U_xH_y^-/U_xD_y^-$ ($x \geq 2$) were observed when backing gas was present. The resulting anions were then extracted with mass selection before entering the photodetachment region.

Anion photoelectron spectroscopy experiments were conducted by crossing a beam of mass-selected actinide hydride negative ions with a fixed-frequency photon beam and energy analyzing the resultant photodetached electrons. The photodetachment process is governed by the energy conservation relationship $h\upsilon$ = EBE + EKE, where $h\upsilon$ is the photon energy, EBE is the electron binding (photodetachment transition) energy, and EKE is the electron kinetic energy. The second (532 nm, 2.33 eV) harmonic of an Nd:YAG laser was used to photodetach electrons from the UH^- and UD^- anions. The PESs were calibrated against the known transitions of Cu^-.[27] The resolution of the magnetic bottle energy analyzer is ∼50 meV at 1 eV EKE.

Computational Methods. Spectroscopic constants including harmonic frequencies (ω_e), anharmonic constants ($\omega_e x_e$), and optimized equilibrium bond lengths were obtained for diatomic UH and the anion UH^- at the CCSD(T)[28−31] level of theory using the MOLPRO program package.[32,33] The calculations were performed using the third-order Douglas−Kroll−Hess Hamiltonian (DKH3)[34−36] with the aug-cc-pVnZ basis set for H[37,38] and the cc-pwCVnZ-DK3 basis set for U[39] (abbreviated as as/aw$n$-DK). The diatomic potential energy curves were obtained by seven single-point calculations distributed around the approximated equilibrium bond length ($r - r_e$ = −0.3, −0.2, −0.1, 0.0, +0.1, +0.3, +0.5 in Bohr). The optimized CCSD(T) energies were extrapolated to the complete basis set (CBS) limit using a mixed Gaussian/exponential[40] for basis sets with n = D, T, Q (awCVnZ-DK)

$$E(n) = E_{CBS} + A \exp[-(n-1)] + B \exp[-(n-1)^2] \quad (1)$$

The valence space included the 6s, 6p, 6d, 5f, and 7s valence electrons on U and the 1s electron on H. Core-valence correlation effects were included by correlating the core−shell 5s, 5p, and 5d electrons. The open-shell calculations were done with the R/UCCSD(T) approach, where a restricted open-shell Hartree−Fock calculation was performed and the spin constraint was then relaxed in the coupled-cluster calculation.[30,41−43]

In order to better describe the low-lying excited states of UH/UH^-, the complete active space self-consistent field (CASSCF)[44,45] approach was used to represent each lowest spin-free state, ΛS, followed by second-order perturbation theory (CASPT2)[46,47] calculations and a treatment of spin−orbit coupling by the state interacting method. The atomic basis functions used in the expansion of the molecular orbitals were the aug-cc-pVnZ basis set[37,48] for hydrogen and the cc-pVnZ-PP basis sets[20,39] for uranium, for n = D, T, and Q. The U basis set includes a small-core energy consistent 60-electron effective core potential (abbreviated as PP) optimized in a multiconfigurational Dirac−Hartree−Fock calculation. These calculations were carried out in the highest Abelian point group available, C_{2v}, for both molecules. Expectation values of L_z^2 were calculated to ensure that both degenerate components of each Λ were correctly accounted for.

The identity of the relevant spin-free states that may contribute to the final relativistic states was determined by the molecular states arising from the coupling between the lowest atomic asymptotes. For UH and UH^-, an ionic model was initially adopted in which the H^- anion is treated as closed

https://doi.org/10.1021/acs.jpca.2c03115
J. Phys. Chem. A 2022, 126, 4432−4443

shell species and U^+ ($^4I_{9/2}$, $5f^37s^2$) and U^0 (^5L, $5f^36d^17s^2$) determined the resulting electronic states. For U^+H^-, the coupling yields quartet ($S = 3/2$) and sextet ($S = 5/2$) low-lying states, and for U^0H^-, it corresponds to a manifold of septets ($S = 3$) through singlet ($S = 0$) states. For the latter, singlets and triplets were found to lie very high in energy; thus, only quintets and septets were calculated. Initially, the CASSCF active space for UH comprised five electrons in 12 orbitals ($4 \times a_1$, $3 \times b_1$, $3 \times b_2$, and $2 \times a_2$), similar to the approach used previously by Cao et al.[19] for this molecule. However, this space failed to describe the states of UH^- and the $6d_z^2$ orbital had to be included. The final active space included five electrons in 13 orbitals ($5 \times a_1$, $3 \times b_1$, $3 \times b_2$, and $2 \times a_2$) that had predominantly U 5f, 6d, and 7s character, and the lower-energy U 5s, 5p, 5d, 6s, 6p, and H 1s orbitals were constrained to be doubly occupied. In the case of UH^-, six electrons in 13 orbitals were included giving a (6/13) CASSCF. In order to generate a common set of molecular orbitals, the ΛS electronic states were state averaged for both species.

On top of the CASSCF -order wavefunction, second-order multiconfigurational perturbation theory (CASPT2) calculations were carried out using the same active space of the preceding calculation to recover dynamical correlation effects. In this step, multiple states are calculated using a Fock operator constructed from a state-averaged density matrix and the zeroth-order Hamiltonians for all states are constructed from the same operator. The frozen-core definition in the CASPT2 included 5s, 5p, and 5d orbitals of U. In order to avoid intruder states, an IPEA[49] shift value of 0.28 was used for all states.

The molecular Ω states arising from the spin−orbit coupling were calculated by applying the state interacting method, as implemented in MOLPRO (SO-CASPT2).[50] In this method, the spin−orbit eigenstates are obtained by diagonalizing $H_{el} + H_{SO}$ in a basis of H_{el} eigenstates. The matrix elements of H_{SO} were constructed using the spin−orbit operator from the U PP. Here, the spin−orbit matrix elements have been calculated throughout at the CASSCF level of the theory using the same basis set as used for the diagonal terms, and the diagonal terms of $H_{el} + H_{SO}$ have been replaced with CASPT2 energies. The latter energies for the two components of each molecular state with $\Lambda \neq 0$ were manually averaged when needed to ensure exact degeneracies. After diagonalization of $H_{el} + H_{SO}$, the values of Ω for each molecule were assigned by converting from a Cartesian eigenfunction basis to a spherical basis and then adding the projection of the spin angular momentum S on the diatomic axis, Σ, to Λ to obtain Ω. These calculations were performed using the a*n*-PP basis set at the corresponding optimized aw*n*-DK bond distances, for n = D, T, Q.

The Feller−Peterson−Dixon (FPD)[51−54] method was used to predict the EA and BDEs for UH. The contributions included in the BDE calculations are defined as follows

$$D_0 = \Delta E_{CBS} + \Delta E_{CV} + \Delta E_{SO} + \Delta E_{ZPE} + \Delta E_{Gaunt} \quad (2)$$

where ΔE_{CBS} is the CCSD(T) energy extrapolated to the CBS limit using the aw*n*-DK basis set for n = D, T, and Q, ΔE_{CV} represents the contribution of the additional correlation due to the valence and outer core electrons, ΔE_{SO} accounts for the SO-CASPT2 energy corrections, and ΔE_{ZPE} is the zero-point energy calculated to be $0.5\ \omega_e - 0.25\ \omega_e x_e$ with frequencies obtained from fitting the CCSD(T)/awQ-DK curve.[55] Contributions from the Gaunt term (ΔE_{Gaunt}), which accounts for spin-other-orbit coupling, were obtained by the difference between the four-component Dirac-Coulomb-Gaunt and spin-free Hamiltonian of Dyall[56] calculations using fully uncontracted basis sets, cc-pVDZ-DK3 on U and aug-cc-pVDZ on H. These calculations were carried out using the DIRAC program.[57] For the AEA and IE calculations, higher order correlation effects were calculated using the DKH3 Hamiltonian with the MRCC[58,59] package connected to MOLPRO, where ΔE_T = CCSDT − CCSD(T) with the aT-DK basis sets[60,61] and ΔE_Q = CCSDTQ − CSSDT with the aD-DK basis sets.[62]

A bonding analysis of the UH species was made through the natural population analysis (NPA) results based on the natural bond orbitals (NBOs)[63,64] using NBO7[65,66] and are calculated using the MOLPRO program package at the aD-DK level. All the calculations were performed on Linux clusters at The University of Alabama.

RESULTS AND DISCUSSION

Photoelectron Spectrum of UH^-. The ions UD^-, UC^-, UN^-, UO^-, and UC_2^- were observed in the mass spectra presented in Figure 1. The PES spectra are given in Figure 2

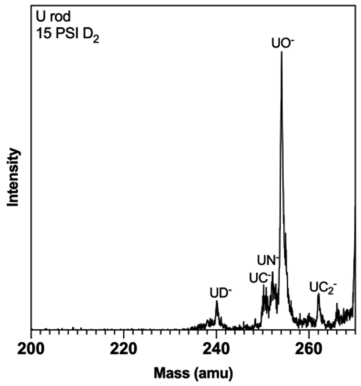

Figure 1. Observed mass spectra using 15 psi of D_2 forming the anions UD^-, UC^-, UN^-, UO^-, and UC_2^-.

with selected EBE values in Table 1. The PES spectra for UH^- and UD^- exhibit a complex spectrum with seven major peaks, ranging from 0.45 to 2.16 eV, and multiple weak peaks are present within this interval.

Electronic Structure Calculations of UH^-. To better understand the PES spectrum, we performed calculations to predict the energetic ordering of low-lying states of UH^- and UH. Table 2 gives the low-lying Ω states at the CASPT2-SO/aQ-PP level with their ΛS composition. Table 3 provides the spectroscopic constants for selected states of UH^-. UH^- has a $^5\Lambda_6$ ground state with a $5f^36d^1$ ($f\delta\ f\pi\ f\varphi\ d\delta$) electronic configuration with the $f\varphi$ orbital highly mixed with the $f\pi$ orbital. The first excited state is predicted to be the $^5K_5$ state ($f\sigma\ f\delta\ f\varphi\ d\delta$) and is higher in energy by 0.054 eV (436 cm^{-1}) at the CASPT2-SO level. At the CCSD(T)/CBS level, these states are almost degenerate with the ^5K state higher in energy by only 54 cm^{-1}. In addition, at the CCSD(T)/CBS level, the second ($^5I_4$) and third excited ($^5H_3$) states have an inverted order compared to the Ω representation results. After the inclusion of spin−orbit effects, the ground state of UH^- lowered its energy by 6912 cm^{-1} (0.857 eV). The equilibrium bond length and harmonic frequency for the ground state were predicted to be 2.144 Å and 1189.2 cm^{-1} at the CCSD(T)/

https://doi.org/10.1021/acs.jpca.2c03115
J. Phys. Chem. A 2022, 126, 4432−4443

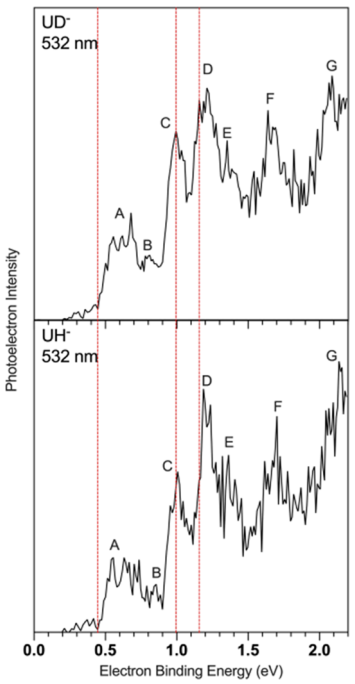

Figure 2. Photoelectron spectra of UD^- (top) and UH^- (bottom) obtained using the second harmonic (532 nm).

Table 1. Electron Binding Energies (EBEs) in eV of the Observed Transitions Using 532 nm Photons To Photodetach the Anions UH^- and UD^-[a]

peaks	UH^- EBE	UD^- EBE
A (onset)	0.462	0.456
A (maxima)	0.551	0.558
B	0.853	0.814
C	1.008	0.998
D	1.190	1.157
E	1.371	1.357
F	1.703	1.640
G	2.158	2.069

[a]Collected using the second harmonic of a Nd:YAG laser (532 nm = 2.33 eV). The error bars on the peaks are ±0.013 eV.

CBS limit obtained by extrapolating the total energies to obtain the potential energy curve at the CBS limit, respectively.

Electronic Structure Calculations of UH. Table 4 gives the low-lying Ω states at the CASPT2-SO/aQ-PP level with their ΛS composition. Table 5 shows the spectroscopic constants for selected states for UH. There are 62 quartet and sextet states within 2.0 eV. The ground state of UH is predicted to be $^4I_{9/2}$ ($5f^37s^2$), which has the unpaired f electrons in the $f\varphi$ $f\delta$ $f\pi$ orbitals, in agreement with the ground state of the U^+ atom ($^4I_{9/2}$). The low-lying states of UH arise from lowering the atomic orbital angular momentum (M_L) of the ^4I (U^+) atomic state yielding the observed H, Γ, Φ, Δ, Π, and Σ states. The lowest excited state ($^4H_{7/2}$) of UH has the $f\varphi$ $f\delta$ $f\sigma$ electronic configuration and is higher in energy by only 0.014 eV (113 cm^{-1}). Likewise, the second excited state, identified as $^4\Gamma_{5/2}$, has a lower angular momentum configuration $f\varphi$ $f\pi$ $f\sigma$ and is only 0.027 eV (218 cm^{-1}) higher than the ground state. These are consistent with the expected ordering of the substates of U^+. The same energetic order of states is observed at the CCSD(T) level, but the $^4H_{7/2}$ state is now higher by 0.026 eV (210 cm^{-1}) and the $^4\Gamma_{5/2}$ state is higher by 0.195 eV (1573 cm^{-1}). The equilibrium bond length and harmonic frequency for the ground state were predicted to be 2.016 Å and 1480.5 cm^{-1} at the CCSD(T)/CBS limit, respectively, in agreement with the previous report by Cao et al.[19] (2.008 Å, 1501 cm^{-1}) using the MRCI-SO all-electron DKH method for the same electronic state. Note that addition of an electron to UH to form UH^- increases the bond distance by 0.13 Å and decreases ω_e by 280 cm^{-1}.

Table 2. Low-Lying States of UH^- at the CASPT2/aq-pp + SO Level[a]

state	Ω	ΔE (eV)	ΛS composition
$^5\Lambda_6$	6	0.000	81% $^5\Lambda$ + 15% ^5K + 2% ^5I
$^5K_5$	5	0.054	68% ^5K + 25% ^5I + 5% ^5H
$^5I_4$	4	0.140	63% ^5I + 30% ^5H + 3% $^5\Gamma$
$^5H_3$	3	0.303	72% ^5H + 27% $^5\Gamma$
$^5\Lambda_7$	7	0.345	73% $^5\Lambda$ + 22% ^5K + 2% ^5I
$^5K_6$	6	0.382	43% ^5K + 32% ^5I + 15% $^5\Lambda$ + 2% ^5H
$^5H_5$	5	0.450	37% ^5H + 27% ^5I + 25% ^5K + 10% $^5\Gamma$
$^5\Gamma_4$	4	0.618	34% $^5\Gamma$ + 33% ^5H + 32% ^5I
$^5\Gamma_6$	6	0.644	100% $^5\Gamma$
$^7M_6$	6	0.691	85% ^7M + 12% $^7\Lambda$
$^5\Lambda_8$	8	0.728	73% $^5\Lambda$ + 23% ^5K + 2% ^5I
$^5K_7$	7	0.751	37% ^5K + 35% ^5I + 21% $^5\Lambda$ + 7% ^5H
$^5H_6$	6	0.786	38% ^5H + 31% ^5K + 15% ^5I + 12% $^5\Gamma$
$^7\Lambda_5$	5	0.831	79% $^7\Lambda$ + 19% ^7K
$^5I_5$	5	0.923	40% ^5I + 37% $^5\Gamma$ + 16% ^5H + 5% ^5K
$^7M_7$	7	0.955	76% ^7M + 19% $^7\Lambda$
$^5\Gamma_3$	3	1.009	73% $^5\Gamma$ + 27% ^5H
$^7K_4$	4	1.023	97% ^7K
$^7\Lambda_6$	6	1.091	57% $^7\Lambda$ + 26% ^7K + 12% ^7M
$^5\Lambda_9$	9	1.155	81% $^5\Lambda$ + 18% ^5K
$^5K_8$	8	1.163	45% ^5K + 30% ^5I + 21% $^5\Lambda$ + 4% ^7M
$^5H_7$	7	1.182	38% ^5H + 34% ^5K + 23%
$^5\Gamma_4$	4	1.212	44% $^5\Gamma$ + 38% ^5I + 9% ^5H + 8% ^5K
$^7M_8$	8	1.235	68% ^7M + 23% $^7\Lambda$ + 4% $^5\Lambda$
$^5\Gamma_4$	4	1.297	59% $^5\Gamma$ + 37% ^5H
$^7K_5$	5	1.352	79% ^7K + 18% $^7\Lambda$
$^7\Lambda_7$	7	1.520	48% $^7\Lambda$ + 31% ^7K + 19% ^7M
$^5\Gamma_5$	5	1.531	51% $^5\Gamma$ + 41% ^5H + 8% ^5I

[a]At the UH^- ($^5\Lambda$) optimized CCSD(T)/awQ-DK geometry.

The lowest-lying sextet state ($^6\Lambda_{11/2}$) is located 0.302 eV (2436 cm^{-1}) above the ground state. The energetic profile of the Ω states of UH resulting from the ΛS quartet and sextet states is illustrated in Figure 3. Potential energy curves were obtained by a seven-point fit procedure around the optimized CCSD(T)/awQ-DK equilibrium distance.[55] Table 6 contains the calculated rovibrational constants with adiabatic excitation energies (T_e) < 7000 cm^{-1}. In general, the r_e values are smaller and the frequencies slightly larger than the ones in Table 5. The interaction of several states between 3000 and 3500 cm^{-1} leads to more anharmonic potential curves as evidenced by the vibrational constants. The T_e values for the five lowest-lying states (Ω = 9/2, 7/2, 5/2, 3/2, 1/2) are nearly the same as the vertical energies collected in Table 4, as they originate from quartet states with very similar bond lengths.

The inclusion of spin−orbit effects leads to the $^4I_{9/2}$ and $^4H_{7/2}$ states being very close energetically at the MR-PT2 level, differing from what was predicted at the CCSD(T) level.

https://doi.org/10.1021/acs.jpca.2c03115
J. Phys. Chem. A 2022, 126, 4432−4443

Table 3. Spectroscopic Properties of Low-Lying States of the Anion UH^- at the CCSD(T) Level

ΛS state	basis set	T_e (eV)	T_e (cm^{-1})	r_e (Å)	B_e (cm^{-1})	ω_e (cm^{-1})	$\omega_e x_e$ (cm^{-1})
$^5\Lambda$	awD-DK	0	0	2.172	3.560	1153.4	36.7
	awT-DK	0	0	2.160	3.602	1170.9	20.0
	awQ-DK	0	0	2.150	3.635	1182.0	6.2
	CBS	0	0	2.144	3.655	1189.2	0.25
^{5}K	awD-DK	−0.017	−136	2.164	3.588	1153.9	24.0
	awT-DK	−0.002	−19	2.156	3.614	1174.8	21.5
	awQ-DK	0.003	27	2.148	3.639	1190.5	22.7
	CBS	0.007	54				
^{5}H	awD-DK	0.027	218	2.169	3.571	1146.2	28.6
	awT-DK	0.028	229	2.155	3.616	1168.2	20.8
	awQ-DK	0.029	238	2.146	3.648	1182.7	19.3
	CBS	0.030	244				
^{5}I	awD-DK	0.049	400	2.167	3.578	1154.5	29.7
	awT-DK	0.056	451	2.156	3.615	1174.5	22.6
	awQ-DK	0.058	465	2.147	3.644	1195.2	31.5
	CBS	0.059	472				

Similar results were found by Bross and Peterson[7] at the CASPT2-SO/CBS for UCl, which has a $^4H_{7/2}$ state only 0.009 eV (76 cm^{-1}) above the ground state ($^4I_{9/2}$). Cao et al.[19] reported vertical excitation energies of 0.039 and 0.056 eV for the $^4H_{7/2}$ and $^4\Gamma_{5/2}$ states, respectively, for UH, slightly higher than the ones predicted in the current work. At the CASPT2-SO/aQ-PP level at the optimized UH (^{4}I) CCSD(T)/awQ-DK geometry, the spin−orbit correction of the UH ground state ($^4I_{9/2}$) is 5782 cm^{-1}. As shown in Table 4, the ground state is well described by a single ΛS state, consisting of 78% ^{4}I and 18% ^{4}H, whereas the $^4H_{7/2}$ and $^4\Gamma_{5/2}$ states present considerable admixtures from other ΛS states.

The results for UH are very similar to those for UF and UCl,[7] as UF has a $^4I_{9/2}$ ground state composed of the 81% ^{4}I + 16% ^{4}H mixture, whereas for UCl, it consists of 77% ^{4}I and 19% ^{4}H. We note that only a few states are reasonably described by a single ΛS, with most excited states being highly mixed.

Electron Detachment Energies. We first discuss the AEA as we will build the computed photodetachment energy ordering from this starting point. The FPD components for the AEA and the ionization energy (IE) are collected in Table 7. The AEAs were obtained by taking the energy differences between the ground states of UH^- ($^5\Lambda_6$) and UH ($^4I_{9/2}$). A value of 0.468 eV was calculated for the AEA of UH, including a contribution of 0.14 eV for spin−orbit effects from the SO-CASPT2 calculation, which is added to the CCSD(T)/CBS value of 0.303 eV. The Gaunt correction is 0.013 eV, and that for higher order correlation corrections is 0.011 eV up through CCSDTQ. The CASPT2-SO/aQ-PP EA is 0.519 eV. An experimental value of 0.462 eV for AEA from the onset is in good agreement with both values. For comparison, ThH has a SO correction of 0.069 eV for the EA, and EA(ThH) is 0.36 eV higher than EA(UH).[25] The EA for the uranium atom was determined experimentally[5] to be 0.31497(9) eV, whereas at the CCSD(T) level plus a full four component spin−orbit coupling correction, a value of 0.232 eV was obtained.[6] For EA(Th), there is better agreement between the experiment, 0.607690(60) eV,[67] and the high level calculated values of 0.599,[62] 0.59,[68] and 0.565 eV.[6]

The VDE from the UH ($^4I_{9/2}$) energy at the UH^- ($^5\Lambda_6$) geometry is 0.056 eV greater than the AEA at the CCSD(T)/CBS level. Adding 0.056 eV to the best estimate of the AEA including the SO corrections and excluding the contribution of ΔE_{ZPE} results in a VDE of 0.506 eV (Tables 7 and 8). The predicted adiabatic and vertical electron affinities are consistent with the peaks shown in the experimental PES spectrum (Figure 2 and Table 1). The first large maximum peak (A) is observed at 0.551 eV for UH^- and 0.558 eV for UD^-. Five VDEs are predicted in the range of 0.50 to 0.57 eV, consistent with the first experimental peak. In addition, there could be other peaks between the onset and the first peak due to the

Table 4. Energies and ΛS Composition of the Low-Lying States of UH at the CASPT2/aQ-PP + SO Level[a]

state	Ω	ΔE (eV)	ΛS composition
$^4I_{9/2}$	4.5	0.000	78% ^{4}I + 18% ^{4}H + 3% $^4\Gamma$
$^4H_{7/2}$	3.5	0.014	58% ^{4}H + 32% $^4\Gamma$ + 9% $^4\Phi$
$^4\Gamma_{5/2}$	2.5	0.027	45% $^4\Gamma$ + 37% $^4\Phi$ + 16% $^4\Delta$
$^4\Delta_{3/2}$	1.5	0.052	39% $^4\Delta$ + 31% $^4\Phi$ + 23% $^4\Pi$ + 7% $^4\Sigma$
$^4\Pi_{1/2}$	0.5	0.060	49% $^4\Pi$ + 32% $^4\Sigma$ + 20% $^4\Delta$
$^6\Lambda_{11/2}$	5.5	0.302	80% $^6\Lambda$ + 17% ^{6}K + 3% ^{6}I
$^6K_{9/2}$	4.5	0.343	66% ^{6}K + 26% ^{6}I + 6% ^{6}H
$^4I_{11/2}$	5.5	0.377	73% ^{4}I + 23% ^{4}H + 3% $^4\Gamma$
$^4\Gamma_{9/2}$	4.5	0.384	36% $^4\Gamma$ + 36% ^{4}H + 18% ^{4}I + 9% Φ
$^4\Phi_{7/2}$	3.5	0.401	38% $^4\Phi$ + 32% ^{4}H + 15% $^4\Delta$ + 14% $^4\Gamma$
$^4\Gamma_{5/2}$	2.5	0.416	39% $^4\Gamma$ + 35% $^4\Delta$ + 23% $^4\Pi$ + 3% $^4\Phi$
$^6I_{7/2}$	3.5	0.417	58% ^{6}I + 31% ^{6}H + 8% $^6\Gamma$
$^4\Phi_{3/2}$	1.5	0.423	42% $^4\Phi$ + 32% $^4\Sigma$ + 26% $^4\Pi$
$^4\Delta_{1/2}$	0.5	0.438	43% $^4\Delta$ + 42% $^4\Pi$ + 15% $^4\Sigma$
$^6H_{5/2}$	2.5	0.538	59% ^{6}H + 33% $^6\Gamma$ + 7% $^6\Phi$
$^6\Lambda_{13/2}$	6.5	0.580	69% $^6\Lambda$ + 25% ^{6}K + 5% ^{6}I
$^6K_{11/2}$	5.5	0.607	37% ^{6}K + 33% ^{6}I + 17% $^6\Lambda$ + 10% ^{6}H
$^6H_{9/2}$	4.5	0.666	36% ^{6}H + 26% ^{6}K + 21% ^{6}I + 14% $^6\Gamma$
$^6\Gamma_{3/2}$	1.5	0.741	72% $^6\Gamma$ + 27% $^6\Phi$
$^6\Gamma_{7/2}$	3.5	0.777	37% $^6\Gamma$ + 33% ^{6}I + 16% ^{6}H + 12% $^6\Phi$
$^4I_{13/2}$	6.5	0.819	79% ^{4}I + 19% ^{4}H
$^4H_{11/2}$	5.5	0.826	41% ^{4}H + 34% $^4\Gamma$ + 24% ^{4}I
$^4\Phi_{9/2}$	4.5	0.838	41% $^4\Phi$ + 38% ^{4}H + 18% $^4\Gamma$ + 3% ^{4}I
$^4\Delta_{7/2}$	3.5	0.854	45% $^4\Delta$ + 41% $^4\Gamma$ + 8% ^{4}H + 5% $^4\Phi$
$^4\Pi_{5/2}$	2.5	0.865	47% $^4\Pi$ + 39% $^4\Phi$ + 14% $^4\Gamma$
$^4\Sigma_{3/2}$	1.5	0.871	43% $^4\Sigma$ + 31% $^4\Delta$ + 22% $^4\Phi$ + 3% $^4\Pi$
$^4\Pi_{1/2}$	0.5	0.883	59% $^4\Pi$ + 30% $^4\Delta$ + 11% $^4\Sigma$
$^6\Lambda_{15/2}$	7.5	0.886	65% $^6\Lambda$ + 29% ^{6}K + 6% ^{6}I
$^6I_{13/2}$	6.5	0.900	34% ^{6}I + 25% $^6\Lambda$ + 24% ^{6}K + 11% ^{6}H
$^6H_{11/2}$	5.5	0.938	35% ^{6}H + 34% ^{6}K + 17% $^6\Gamma$ + 8% ^{6}I
$^6H_{5/2}$	2.5	0.990	37% ^{6}H + 34% $^6\Phi$ + 29% $^6\Gamma$
$^6I_{9/2}$	4.5	1.025	38% ^{6}I + 35% $^6\Gamma$ + 17% $^6\Phi$ + 6% ^{6}K
$^6\Phi_{1/2}$	0.5	1.094	100% $^6\Phi$
$^6I_{15/2}$	7.5	1.220	37% ^{6}I + 29% $^6\Lambda$ + 24% ^{6}K + 9% ^{6}H
$^6H_{7/2}$	3.5	1.224	42% ^{6}H + 37% $^6\Phi$ + 11% $^6\Gamma$ + 7% ^{6}I

[a]At the UH (^{4}I) optimized CCSD(T)/awQ-DK geometry.

https://doi.org/10.1021/acs.jpca.2c03115
J. Phys. Chem. A 2022, 126, 4432−4443

Table 5. Spectroscopic Properties of Low-Lying States of UH at the CCSD(T) Level

ΛS state	basis set	T_e (eV)	T_e (cm^{-1})	r_e (Å)	B_e (cm^{-1})	ω_e (cm^{-1})	$\omega_e x_e$ (cm^{-1})
^{4}I	awD-DK	0	0	2.021	4.111	1475.7	21.0
	awT-DK	0	0	2.021	4.112	1458.2	9.0
	awQ-DK	0	0	2.018	4.125	1471.2	14.4
	CBS	0	0	2.016	4.134	1480.5	18.4
^{4}H	awD-DK	0.026	208	2.021	4.115	1463.9	19.3
	awT-DK	0.019	156	2.018	4.124	1453.0	18.1
	awQ-DK	0.018	147	2.014	4.140	1461.7	14.1
	CBS	0.018	142				
$^4\Gamma$	awD-DK	0.195	1572	2.022	4.109	1483.9	21.2
	awT-DK	0.204	1644	2.021	4.112	1476.9	15.7
	awQ-DK	0.206	1664	2.017	4.130	1489.6	13.0
	CBS	0.208	1677				
$^4\Delta$	awD-DK	0.290	2336	2.021	4.114	1464.2	20.6
	awT-DK	0.311	2512	2.024	4.101	1448.7	12.5
	awQ-DK	0.322	2601	2.022	4.111	1461.9	20.2
	CBS	0.329	2655				

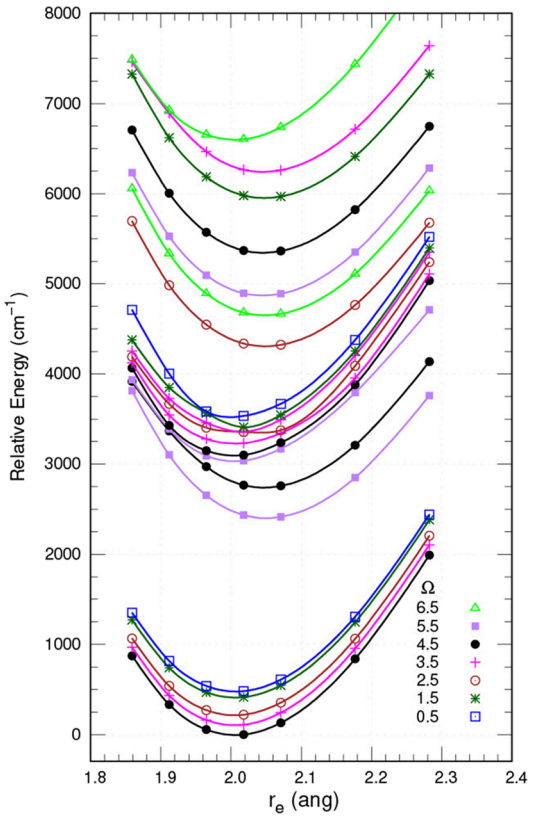

Figure 3. SO-CASPT2/aQ-PP potential energy curves for the low-lying Ω states of UH.

Table 6. SO-CASPT2/aQ-PP Spectroscopic Parameters for the Low-Lying Ω States of UH

ΛS state	T_e (eV)	T_e (cm^{-1})	r_e (Å)	B_e (cm^{-1})	ω_e (cm^{-1})	$\omega_e x_e$ (cm^{-1})
$^4I_{9/2}$	0.000	0	2.006	4.174	1525.5	17.2
$^4H_{7/2}$	0.014	109	2.005	4.183	1523.1	17.2
$^4\Gamma_{5/2}$	0.027	220	2.005	4.185	1516.6	17.0
$^4\Delta_{3/2}$	0.051	415	2.006	4.181	1514.2	16.9
$^4\Pi_{1/2}$	0.060	483	2.007	4.177	1515.1	17.0
$^6\Lambda_{11/2}$	0.298	2404	2.050	4.001	1479.0	33.8
$^6K_{9/2}$	0.339	2735	2.046	4.016	1454.0	18.9
$^4I_{11/2}$	0.376	3035	2.005	4.188	1551.4	77.4
$^4\Gamma_{9/2}$	0.384	3097	2.004	4.192	1535.7	28.7
$^4\Phi_{7/2}$	0.401	3234	2.005	4.176	1415.0	28.7
$^4\Gamma_{5/2}$	0.417	3359	2.008	4.170	1344.8	5.4
$^6I_{7/2}$	0.417	3364	2.011	4.160	1561.7	24.2
$^4\Phi_{3/2}$	0.423	3411	2.005	4.184	1534.8	14.7
$^4\Delta_{1/2}$	0.439	3538	2.005	4.154	1516.2	20.0
$^6H_{5/2}$	0.535	4311	2.048	4.009	1457.7	18.2
$^6\Lambda_{13/2}$	0.577	4655	2.048	4.009	1466.4	17.0
$^6K_{11/2}$	0.604	4875	2.045	4.020	1467.2	16.9
$^6H_{9/2}$	0.663	5350	2.046	4.019	1464.0	17.0
$^6\Gamma_{3/2}$	0.739	5958	2.047	4.016	1442.2	18.9
$^6\Gamma_{7/2}$	0.773	6235	2.049	4.006	1479.9	54.9
$^4I_{13/2}$	0.819	6603	2.005	4.185	1523.8	29.5

first low-lying $^5K_5$ excited electronic state of UH^- at 0.053 eV lowering the VDE.

Continuing the assignment of excited states of UH in the PES spectrum, our calculated results show that there are two states between the experimental **A** and **B** maxima at 0.75 and 0.80 eV. There are two states near 0.88 eV that can be assigned to the **B** experimental peak and an additional five states between 0.89 and 0.94 eV, which could be part of this peak. The intense experimental peak **C** with an EBE of 1.008 eV (UH^-) is consistent with the calculated $^6H_{5/2}$ state. In addition, there are predicted peaks at 1.04, 1.07, and 1.13 eV. There are two $^6\Gamma$ states consistent with the experimental EBE **D** peak of 1.190 eV for UH^-. From 1.32 to 1.41 eV, there are 10 predicted states, which can account for the experimental **E** peak at 1.371 eV. From 1.45 to 1.56 eV, there are three states. The experimental **F** peak is at 1.703 eV, and there are five predicted states between 1.68 and 1.75 eV, which can account for this peak. The next assigned experimental peak is the **G** peak at 2.158 eV. Between 1.84 and 2.11 eV, there are 16 states and the higher values of these states at 2.09 and 2.1 eV could account for the observed peak at 2.16 eV. There are then an additional eight states between 2.27 and 2.49 eV.

Thermochemistry. The BDE of UH was obtained as follows. Direct calculation of the BDE(UH) to obtain the heat of formation following the FPD approach is not straightforward as accurate calculations of the U atom are difficult due to its $7s^26d^15f^3$ ground state. Rather than directly calculating the BDE using the U atom, we can calculate the BDE from the ionization potential of UH because U^+ with a $5f^37s^2$ configuration has only open-shell 5f orbitals. This makes the calculations simpler as we do not have to consider coupling to the 6d orbital as would be found in U. The BDE of UH^+ is available from the experiment and from high-level calculations, which are consistent with each other.[23] We redid the calculations of the BDE of UH^+ using the FPD approach

https://doi.org/10.1021/acs.jpca.2c03115
J. Phys. Chem. A 2022, 126, 4432−4443

Table 7. FPD Components for the EA and IP at 0 K with DK Basis Sets of UH in eV

neutral	ion	property	awQ-DK	ΔE_{CBS}[a]	ΔE_{CV}[b]	ΔE_{ZPE}[b]	ΔE_{SO}[c]	ΔE_{Gaunt}[d]	ΔE_{CCSDT}[e]	ΔE_{CCSDTQ}[f]	final (0 K)
UH ($^4I_{9/2}$)	UH^- ($^5\Lambda_6$)	AEA	0.278	0.303	−0.017	0.018	0.140	0.013	0.047	−0.036	0.468
		VDE[g]	0.337	0.359							0.506[h]
UH ($^4I_{9/2}$)	UH^+ ($^5I_4$)	IE	6.048	6.054	0.029	0.010	−0.032	0.031	0.009	0.015	6.116

[a]CCSD(T) value extrapolated to the CBS limit using aw*n*-DK basis sets for *n* = D, T, Q. [b]CCSD(T)/awQ-DK. [c]SO-CASPT2 values: UH^- = 0.857 eV (6912 cm^{-1}), UH = 0.717 eV (5781 cm^{-1}), UH^+ = 0.749 eV (6040 cm^{-1}). [d]Fully uncontracted cc-pVDZ-DK3. [e]ΔE_T = CCSDT − CCSD(T). [f]ΔE_Q = CCSDTQ − CCSDT. [g]UH ($^4I_{9/2}$) at UH^- ($^5\Lambda_6$) geometry for each level of theory. [h]Value does not include a ZPE correction but includes the same other corrections as calculated for the AEA.

Table 8. Calculated VDEs at the CASPT2/aQ-PP + SO Level[a]

state	VDE	state	VDE
$^4I_{9/2}$	0.506	$^6\Phi_{1/2}$	1.558
$^4H_{7/2}$	0.520	$^6I_{15/2}$	1.689
$^4\Gamma_{5/2}$	0.533	$^6H_{7/2}$	1.690
$^4\Delta_{3/2}$	0.556	$^6\Lambda_{17/2}$	1.690
$^4\Pi_{1/2}$	0.564	$^6H_{13/2}$	1.711
$^6\Lambda_{11/2}$	0.763	$^6I_{11/2}$	1.753
$^6K_{9/2}$	0.807	$^4I_{15/2}$	1.843
$^4I_{11/2}$	0.880	$^4H_{13/2}$	1.854
$^4\Gamma_{9/2}$	0.883	$^4\Gamma_{11/2}$	1.856
$^4\Phi_{7/2}$	0.892	$^4\Phi_{9/2}$	1.856
$^4\Gamma_{5/2}$	0.908	$^4\Phi_{7/2}$	1.865
$^6I_{7/2}$	0.923	$^6\Phi_{3/2}$	1.882
$^4\Phi_{3/2}$	0.929	$^4\Delta_{5/2}$	1.896
$^4\Delta_{1/2}$	0.944	$^4\Pi_{1/2}$	1.900
$^6H_{5/2}$	1.000	$^6\Phi_{3/2}$	1.902
$^6\Lambda_{13/2}$	1.043	$^6H_{9/2}$	1.910
$^6K_{11/2}$	1.073	$^6K_{17/2}$	2.051
$^6H_{9/2}$	1.131	$^6H_{15/2}$	2.054
$^6\Gamma_{3/2}$	1.205	$^6\Lambda_{19/2}$	2.064
$^6\Gamma_{7/2}$	1.242	$^6\Gamma_{13/2}$	2.080
$^4I_{13/2}$	1.324	$^6\Phi_{5/2}$	2.090
$^4H_{11/2}$	1.334	$^6\Phi_{11/2}$	2.109
$^4\Phi_{9/2}$	1.347	$^6\Phi_{7/2}$	2.276
$^4\Delta_{7/2}$	1.351	$^6\Gamma_{9/2}$	2.413
$^4\Pi_{5/2}$	1.363	$^6I_{17/2}$	2.440
$^4\Sigma_{3/2}$	1.370	$^6H_{15/2}$	2.440
$^4\Pi_{1/2}$	1.372	$^6K_{19/2}$	2.451
$^6\Lambda_{15/2}$	1.379	$^6H_{13/2}$	2.461
$^6I_{13/2}$	1.391	$^6\Lambda_{21/2}$	2.475
$^6H_{11/2}$	1.406	$^6\Gamma_{11/2}$	2.492
$^6H_{5/2}$	1.454		
$^6I_{9/2}$	1.492		

[a]At the optimized UH^- ($^5\Lambda$) CCSD(T)/awQ-DK geometry.

outlined in the current work with the components in Table 9. We note that the SO correction for UH^+ is 6040 cm^{-1} and that for U^+ is 6704 cm^{-1} obtained at the CASPT2-SO level. The SO value for U^+ is consistent with a value of 6851 cm^{-1} obtained from the expression $\sum_J(2J + 1)E(J)/\sum_J(2J + 1)$ using the ground state values for $E(J)$ for U^+.[3] We obtain a value of 235.5 kJ/mol for the BDE(UH^+), which can be compared to an experimental value of 239.3 ± 5.8 kJ/mol (2.48 ± 0.06 eV) and a calculated value of 234.5 kJ/mol at the CCSD(T)/CBS/cc-pwCVnZ-DK3 level.[23] The calculated IE of UH is 6.12 eV at the FPD level. In combination with the heat of formation of UH^+, which can be readily obtained from the experimental IE of U, we can obtain the values for UH, UH^+, and UH^- given in Table 10. For UH^-, ΔH_f° was obtained using the AEA and the heat of formation of UH. Standard heats of formation at 298 K were calculated using the approach described by Curtiss et al.[69] using 6.36[66] and 4.23 kJ/mol[64] for the thermal corrections of U and H, respectively.

Another way to obtain the heat of formation of UH is by reaction 3 building on our work

$$UH + WF_6 \rightarrow UF_6 + WH \quad (3)$$

on UCl_6.[70] We chose reaction 3 as the nominal oxidation states are the same. $\Delta H_f^\circ{}_{0K}$ of UF_6 is −2142.5 kJ/mol,[63] obtained from the experimental value reported by Guillaumont et al.[71] of −2148.6 ± 1.9 kJ/mol at 298 K with the thermal correction for 0 to 298 K from Wagman et al.[72] of 6.1 kJ/mol. The FPD value[73] for $\Delta H_f^\circ{}_{0K}(WF_6)$ is −1763.1 kJ/mol; thus, we can

https://doi.org/10.1021/acs.jpca.2c03115
J. Phys. Chem. A 2022, 126, 4432−4443

Table 9. FPD Components for the BDE of UH^+ ($UH^+ \rightarrow U^+ + H$) in kJ/mol

component	energy
awd-DK	232.0
awt-DK	239.5
awq-DK	244.7
ΔE_{CBS}[a]	248.0
ΔE_{CV}	8.1
ΔE_{SO}	−7.94
ΔE_{Gaunt}	−2.91
ΔE_{ZPE}[b]	−9.76
D_0 (0 K)	235.5

[a]CCSD(T) value extrapolated to the CBS limit using aw*n*-DK basis sets for *n* = D, T, Q. [b]CCSD(T)/awQ-DK.

Table 10. Heats of Formation ($\Delta H_f°$) and BDEs (D_0) of $UH^{0/-}$ in kJ/mol

diatomic	$\Delta H_f°$(0 K)[a]	$\Delta H_f°$(298 K)[a]	D_0[b]
UH	523.5	521.6	225.5
UH^-	478.4	476.5	197.9[c]
UH^+	1113.6	1111.7	235.5[d]

[a]We estimate an error of ±10 kJ/mol of the heats of formation predominantly due to the error bar for the heat of formation of the U atom. [b]We estimate an error of ±5 kJ/mol for the value of D_0 predominantly due to potential errors in the spin−orbit calculations. [c]To U + H^-. [d]To U^+ + H.

calculate $\Delta H_f°$(WH) using the FPD approach. We calculate the heat of formation of WH with respect to the ^7S atomic state of tungsten and then correct it to the ground state by 35.31 kJ/mol (8.44 kcal/mol).[3] At the FPD level (see the Supporting Information for details of the calculation), the BDE for WH is 266.6 kJ/mol giving $\Delta H_f°_{0K}$(WH) = 800.5 kJ/mol. The energy of reaction 3 at the CCSD(T)/CBS level is −81.5 kJ/mol at 0 K giving $\Delta H_f°_{0K}$(UH) = 530.6 kJ/mol, in close agreement with a value of 523.5 kJ/mol from the IE + BDE approach described above. We note that it is critical to include the SO corrections for the MH because the value at the CASPT2-SO/aug-cc-pVQZ-PP level for UH is −69.2 kJ/mol, whereas for WH, it is only −3.3 kJ/mol.

The BDEs (Table 11) for UH and UH^- were calculated from the known atomic heat of formation of U ($\Delta H_f°$(0 K) = 533.0 ± 8 kJ/mol)[66] and the values for H ($\Delta H_f°$(0 K) = 216.034 kJ/mol) and H^- ($\Delta H_f°$(0 K) = 143.264 kJ/mol) from the active thermochemical tables (ATcT).[74−76] The values for all of the metal hydrides in Table 11 were calculated in this work except for ThH taken from our prior work.[25] The BDE for UH is ∼20% weaker than the BDE of ThH even though the bond distances are essentially the same. This can partially be explained by the nonbonding 5f electrons in U having a repulsive interaction with the H^-, and such an interaction is not present in Th. The BDE for UH^- is lower than that for UH, by 30 kJ/mol, whereas the BDE for ThH^- is 7 kJ/mol higher than that for ThH. For the UH^- and ThH^- anions, dissociation leads to M + H^-, not M^- + H, as the EA of H is larger than those of U and Th.[71]

Table 11. M−H, Average M−O, and Average M−F BDEs in kJ/mol

hydride	M−H[a]	oxide	M=O[b]	fluoride	M−F[c]
MoH	230.4	MoO_3	574.5	MoF_6	447.0
WH	238.4	WO_3	641.0	WF_6	512.7
UH	225.5	UO_3	693.3	UF_6	526.3
ZrH	247.0	ZrO_2	692.0	ZrF_4	647.0
HfH	266.6	HfO_2	666.1	HfF_4	657.2
ThH	260.5	ThO_2	777.7	ThF_4	667.1

[a]$D_0{}^0$. Current work unless noted. ThH from ref 25. [b]Average M=O from the oxide. Values for MoO_3, WO_3, ZrO_2, and HfO_2 from ref 65 at the CCSD(T)-PW91/CBS level, UO_3 from ref 66, and ThO_2 from ref 72. [c]Average M−F from the fluoride. Values for MoF_6 from ref 73, WF_6 from ref 68, UF_6 from ref 66, and ZrF_4, HfF_4, and ThF_4 from ref 74.

We can also compare the trends for various bond energies in a column. The BDE for WH is slightly larger than that for MoH, and the UH BDE is the smallest of these three. The trend in BDEs for ZrH (this work) and HfH (this work) is the same as that for MoH and WH, but the ThH BDE[25] falls in between those of ZrH and HfH. We can compare the average MO BDEs from MO_2 and MO_3 as well.[65,66,77] The metals in the +IV oxidation state have higher BDEs than those in the +VI oxidation state. For the +VI MO_3, the BDEs increase from Mo to U, but the +IV oxidation-state BDEs decrease from ZrO_2 to HfO_2 and then substantially increase for ThO_2. The average M−F BDEs for MF_4 and MF_6 increase down the column.[66,68,78,79] The values for MF_4 are larger than those for MF_6 in part due to smaller steric interactions in the former. Thus, the ordering of the BDEs depends on the ligand and the metal oxidation state.

Electronic Structure Analysis. As expected, an examination of the molecular orbitals of UH and UH^- indicates that bonding in these molecules has mostly ionic character. Table 12 shows the NPA charges and population from the natural bond orbital analysis obtained at the AD-DK level for selected low-lying states of UH and UH^-. The interaction of U^+ ($^4I_{9/2}$) with H^- gives rise to the low-lying UH states. The ground state of UH ($^4I_{9/2}$) is well described by the $f\varphi\ f\delta\ f\pi$ electronic configuration with the highest occupied MO of σ symmetry having strongly 5f character. Bonding character is observed for the second highest MO, which is a mixture of the atomic functions $6d_0$ + 7s (U) strongly polarized toward the 1s H. A similar pattern is observed for the $^4H_{7/2}$ ($f\varphi\ f\delta\ f\sigma$) state, which is only 0.014 eV higher in energy than the ground state and is expected to contribute to its ΛS composition (Table 4).

The natural charge for U in UH is +0.71, and that for H is clearly highly negative. These results are consistent with the assignment of an ionic configuration ($U^{+0.71}H^{-0.71}$) for UH. In this case, the U 7s orbitals remain double occupied with about 1.88 e, and the U 5f orbitals have three unpaired electrons (3.0 e) in agreement with the $5f^37s^2$ configuration associated with the U^+(^4I_u) lowest atomic asymptote. There are 0.38 electrons in the U 6d, and there are 1.68 electrons in the H 1s orbital. The populations for the $^4I_{9/2}$ and $^4H_{7/2}$ states of UH are basically the same. As the U^+ (^6L_u) atomic asymptote is higher by only 289 cm^{-1}, we calculated the atomic charges for the first sextet excited state, $^6\Lambda_{11/2}$. The atomic charges slightly change to 0.677 (U) and −0.677 (H) as compared to the quartet states. The 6d population increases by almost one electron to 1.32 e, and the 7s orbital decreases to 0.98 e corresponding to the expected $5f^36d^17s^1$ U configuration.

The bonding in UH^- results from the interaction of U ($5f^36d^17s^2$) with the closed shell H^- ($1s^2$). The natural charges calculated for U are −0.12 e in UH^-, whereas for H, there is a population of −0.88 e, so most of the additional electron goes

https://doi.org/10.1021/acs.jpca.2c03115
J. Phys. Chem. A 2022, 126, 4432−4443

Table 12. NBO/HF Charges (q) and U Population at the HF-aD-DK Level

	q(U)	q(H)	5f[a]	6d[a]	7s[a]	7p[a]	H 1s[a]
UH							
$^4I_{9/2}$	0.711	−0.711	3.02 (2.99/0.02)	0.38 (0.20/0.18)	1.88 (0.94/0.94)	0.03 (0.01/0.01)	1.68 (0.84/0.84)
$^4H_{7/2}$	0.710	−0.710	3.02 (3.00/0.02)	0.38 (0.20/0.18)	1.88 (0.94/0.94)	0.03 (0.01/0.01)	1.68 (0.84/0.84)
$^6\Lambda_{11/2}$	0.677	−0.677	2.99 (2.98/0.01)	1.32 (1.23/0.08)	0.98 (0.90/0.08)	0.03 (0.03/0.00)	1.66 (0.84/0.82)
UH^-							
$^5\Lambda_6$	−0.123	−0.877	3.00 (3.00/0.01)	1.18 (1.09/0.09)	1.87 (0.94/0.94)	0.06 (0.03/0.03)	1.79 (0.90/0.90)
$^5K_5$	−0.129	−0.871	2.98 (2.98/0.01)	1.21 (1.12/0.09)	1.88 (0.94/0.94)	0.05 (0.03/0.02)	1.79 (0.89/0.89)

[a]In the order total spin (α spin, β spin).

onto the U. U gains −0.83 e as compared to the U in UH, and H is 0.16 e more negative in UH^- than in UH. In comparison with UH, the additional electron goes into the 6d orbitals with a population of 1.20 e. The 7p population remains very small in UH^- as in UH.

CONCLUSIONS

The UH and UH^- molecules were characterized by high-level electronic structure calculations combined with anion photoelectron spectroscopy experiments to study the interaction of U with this simplest ligand. The ground state of UH is predicted to be $^4I_{9/2}$ ($f\varphi\ f\delta\ f\pi$) at both the SO-CASPT2 and CCSD(T) levels with the $^4H_{7/2}$ excited state only 0.014 eV higher in energy. For UH^-, the ground state is predicted to be $^5\Lambda_6$ with ($f\delta\ f\pi\ f\varphi\ d\delta$) and the first excited state $^5K_5$ higher by 0.054 eV at the CASPT2-SO level. At the CCSD(T) level, the two states are essentially degenerate, which shows the importance of including spin−orbit effects in the assignment of the low-lying states.

At the FPD level, the AEA of UH is calculated to be 0.468 eV, in good agreement with an extrapolated experimental value of 0.462 V. The theoretical value includes a spin−orbit correction of 0.14 eV. At the CASPT2-SO/aQ-PP level, the AEA was calculated to be 0.519 eV. The EA of UH is about 0.17 eV larger than the EA of the U atom, an increase of ∼60%. This is similar to the absolute differences in the electron affinities of Th and ThH. The photodetachment spectrum of UH^- is complicated by the large number of low-lying excited states in UH, which can be accessed in less than 2.0 eV. This again is similar to the situation for ThH^- photodetachment. The vertical EA, obtained at the FPD level, is predicted to be 0.506 eV. The assignments of the excited states of UH up to ∼2.5 eV show consistency with the PES spectrum.

Considering dissociation to U^+ + H, the IE of UH at the FPD level was computed to be 6.116 eV including a small spin−orbit correction of −0.032 eV. The IE is 0.08 eV lower than the experimental IE of U, which suggests that H has only a moderate influence as a ligand on the IE. At the CASPT2-SO level, the IE is estimated to be 6.040 eV.

The BDE of UH was obtained from the calculated IE and heat of formation of UH^+. The BDE of UH^+ is estimated to be 235.5 kJ/mol at the FPD level, including a −7.94 kJ/mol spin−orbit correction, and ΔH_f°(0 K) = 1113.6 kJ/mol. For UH, we obtained a BDE of 225.5 kJ/mol and ΔH_f° (0 K) = 523.5 kJ/mol. These values are essentially the same as the ones obtained from reaction 3. For UH^-, we calculated a BDE of 197.9 kJ/mol with ΔH_f°(0 K) = 478.4 kJ/mol. Compared with ThH, the UH BDE is lower by ∼20%, which can be explained by the presence of the f^3 nonbonding electrons on the U.

The NBO electronic structure analysis is consistent with the $5f^3$ subconfiguration for the bonding of the $UH^{0/-1}$ species and supports the presence of significant ionic character. Considering ionic bonding for UH (U^+H^-), there are 21 spin−orbit states in U^+ below 1 eV, which originate from the $5f^37s^2$, $5f^36d^17s^1$, $5f^36d^2$, and $5f^47s^1$ atomic configurations.[3] If we assume only a covalent bond (UH), there are 19 spin−orbit states in the neutral U, which are mostly associated with the $5f^36d^17s^2$ configuration.[3] Only a few states are derived from $5f^36d^27s^1$ and $5f^47s^2$ up to 1 eV excitation energy.

ASSOCIATED CONTENT

Supporting Information

The Supporting Information is available free of charge at https://pubs.acs.org/doi/10.1021/acs.jpca.2c03115.

Complete citations for refs 32, 33, 57; additional computational results including total energies and associated detachment energies and energy components (PDF)

AUTHOR INFORMATION

Corresponding Authors

Kit H. Bowen − *Department of Chemistry, Johns Hopkins University, Baltimore, Maryland 21218, United States;* orcid.org/0000-0002-2858-6352; Email: kbowen@jhu.edu

David A. Dixon − *Department of Chemistry and Biochemistry, The University of Alabama, Tuscaloosa, Alabama 35401, United States;* orcid.org/0000-0002-9492-0056; Email: dadixon@ua.edu

Authors

Gabriel F. de Melo − *Department of Chemistry and Biochemistry, The University of Alabama, Tuscaloosa, Alabama 35401, United States*

Monica Vasiliu − *Department of Chemistry and Biochemistry, The University of Alabama, Tuscaloosa, Alabama 35401, United States*

Mary Marshall − *Department of Chemistry, Johns Hopkins University, Baltimore, Maryland 21218, United States*

Zhaoguo Zhu − *Department of Chemistry, Johns Hopkins University, Baltimore, Maryland 21218, United States;* orcid.org/0000-0002-4395-9102

Burak A. Tufekci − *Department of Chemistry, Johns Hopkins University, Baltimore, Maryland 21218, United States*

Sandra M. Ciborowski − *Department of Chemistry, Johns Hopkins University, Baltimore, Maryland 21218, United States*

https://doi.org/10.1021/acs.jpca.2c03115
J. Phys. Chem. A 2022, 126, 4432−4443

Moritz Blankenhorn − *Department of Chemistry, Johns Hopkins University, Baltimore, Maryland 21218, United States*

Rachel M. Harris − *Department of Chemistry, Johns Hopkins University, Baltimore, Maryland 21218, United States*

Complete contact information is available at: https://pubs.acs.org/10.1021/acs.jpca.2c03115

Notes

The authors declare no competing financial interest.

■ ACKNOWLEDGMENTS

This work was supported by the U.S. Department of Energy (DOE), Office of Science, Office of Basic Energy Sciences, Heavy Element Chemistry program at Johns Hopkins University (K.H.B., experiment) through Grant Number DE-SC0019317 and at The University of Alabama (D.A.D., computational) through Grant No. DE-SC0018921. D.A.D. thanks the Robert Ramsay Fund at The University of Alabama.

■ REFERENCES

(1) Choppin, G. Actinide Speciation in the Environment. *J. Radioanal. Nucl. Chem.* **2007**, *273*, 695−703.
(2) Petti, D.; Crawford, D.; Chauvin, N. Fuels for Advanced Nuclear Energy Systems. *MRS Bull.* **2009**, *34*, 40−45.
(3) Sansonetti, J. E.; Martin, W. C. Handbook of Basic Atomic Spectroscopic Data. *J. Phys. Chem. Ref. Data* **2005**, *34*, 1559−2259.
(4) Grenthe, I.; Drożdżyński, J.; Fujino, T.; Buck, E. C.; Albrecht-Schmitt, T. E., Wolf, S. F. Uranium. In *The Chemistry of the Actinide and Transactinide Elements*; 3rd ed.; Morss, L. R., Edelstein, N. M., Fuger, J., Eds.; Springer: Dordrecht, The Netherlands, 2006; Vol. *3*; pp 253−698.
(5) Tang, R.; Lu, Y.; Liu, H.; Ning, C. Electron affinity of Uranium and Bound States of Opposite Parity in its Anion. *Phys. Rev. A* **2021**, *103*, No. L050801.
(6) Ciborowski, S. M.; Liu, G.; Blankenhorn, M.; Harris, R. M.; Marshall, M. A.; Zhu, Z.; Bowen, K. H.; Peterson, K. A. The Electron Affinity of the Uranium Atom. *J. Chem. Phys.* **2021**, *154*, 224307.
(7) Bross, D. H.; Peterson, K. A. Theoretical Spectroscopy Study of the Low-Lying Electronic States of UX and UX^+, X= F and Cl. *J. Chem. Phys.* **2015**, *143*, 184313.
(8) Antonov, I. O.; Heaven, M. C. Spectroscopic and Theoretical Investigations of UF and UF^+. *J. Phys. Chem. A* **2013**, *117*, 9684−9694.
(9) Battey, S. R.; Bross, D. H.; Peterson, K. A.; Persinger, T. D.; VanGundy, R. A.; Heaven, M. C. Spectroscopic and Theoretical Studies of UN and UN^+. *J. Chem. Phys.* **2020**, *152*, No. 094302.
(10) Goncharov, V.; Kaledin, L. A.; Heaven, M. C. Probing the electronic structure of UO^+ with high-resolution photoelectron spectroscopy. *J. Chem. Phys.* **2006**, *125*, 133202.
(11) Gagliardi, L.; Roos, B. O. Quantum Chemical Calculations Show that the Uranium Molecule U_2 has a Quintuple Bond. *Nature* **2005**, *433*, 848−851.
(12) Gagliardi, L.; Pyykkö, P.; Roos, B. O. A Very Short Uranium−Uranium Bond: The Predicted Metastable U_2^{2+}. *Phys. Chem. Chem. Phys.* **2005**, *7*, 2415−2417.
(13) Fedorov, D. G.; Nakajima, T.; Hirao, K. An Ab Initio Study of Excited States of U and UF. *J. Chem. Phys.* **2003**, *118*, 4970−4975.
(14) Wang, X.; Andrews, L.; Ma, D.; Gagliardi, L.; Gonçalves, A. P.; Pereira, C. C. L.; Marçalo, J.; Godart, C.; Villeroy, B. Infrared Spectra and Quantum Chemical Calculations of the Uranium-Carbon Molecules UC, CUC, UCH, and $U(CC)_2$. *J. Chem. Phys.* **2011**, *134*, 244313.
(15) Gagliardi, L.; Roos, B. O. Multiconfigurational Quantum Chemical Methods for Molecular Systems Containing Actinides. *Chem. Soc. Rev.* **2007**, *36*, 893−903.
(16) Krauss, M.; Stevens, W. J. Comparative Electronic Structure of a Lanthanide and Actinide Diatomic Oxide: Nd versus U. *Mol. Phys.* **2003**, *101*, 125−130.
(17) Krauss, M.; Stevens, W. J. Electronic Structure of UH, UF, and Their Ions. *J. Comput. Chem.* **1983**, *4*, 127−135.
(18) Roos, B. O.; Malmqvist, P.; Gagliardi, L. Exploring the Actinide-Actinide Bond: Theoretical Studies of the Chemical Bond in Ac_2, Th_2, Pa_2, and U_2. *J. Am. Chem. Soc.* **2006**, *128*, 17000−17006.
(19) Cao, X.; Moritz, A.; Dolg, M. All-electron Douglas−Kroll−Hess and Pseudopotential Study on the Low-lying States of Uranium Hydride UH. *Chem. Phys.* **2008**, *343*, 250−257.
(20) Dolg, M.; Cao, X. Accurate Relativistic Small-core Pseudopotentials for Actinides. Energy Adjustment for Uranium and First Applications to Uranium Hydride. *J. Phys. Chem. A.* **2009**, *113*, 12573−12581.
(21) Souter, P. F.; Kushto, G. P.; Andrews, L.; Neurock, M. Experimental and Theoretical Evidence for the Formation of Several Uranium Hydride Molecules. *J. Am. Chem. Soc.* **1997**, *119*, 1682−1687.
(22) Vent-Schmidt, T.; Andrews, L.; Riedel, S. Reactions of Laser-ablated U atoms with HF: Infrared Spectra and Quantum Chemical Calculations of HUF, UH, and UF in Noble Gas Solids. *J. Phys. Chem. A* **2015**, *119*, 2253−2261.
(23) Zhang, W.-J.; Demireva, M.; Kim, J.; de Jong, W. A.; Armentrout, P. B. Reactions of U^+ with H_2, D_2, and Hd Studied by Guided Ion Beam Tandem Mass Spectrometry and Theory. *J. Phys. Chem. A* **2021**, *125*, 7825−7839.
(24) Cox, R. M.; Armentrout, P. B.; de Jong, W. A. Reactions of Th^+ + H_2, D_2, and HD Studied by Guided Ion Beam Tandem Mass Spectroscopy and Quantum Chemical Calculations. *J. Phys. Chem. B* **2016**, *120*, 1601−1614.
(25) Vasiliu, M.; Peterson, K. A.; Marshall, M.; Zhu, Z.; Tufekci, B. A.; Bowen, K. H.; Dixon, D. A. Interaction of Th with $H^{0/-/+}$: Combined Experimental and Theoretical Thermodynamic Properties. *J. Phys. Chem. A* **2022**, *126*, 198−210.
(26) Gerhards, M.; Thomas, O. C.; Nilles, J. M.; Zheng, W.-J.; Bowen, K. H. Cobalt-Benzene Cluster Anions: Mass Spectrometry and Negative Ion Photoelectron Spectroscopy. *J. Chem. Phys.* **2002**, *116*, 10247−10252.
(27) Ho, J.; Ervin, K. M.; Lineberger, W. C. Photoelectron spectroscopy of metal cluster anions: Cu_n^-, Ag_n^-, and Au_n^-. *J. Chem. Phys.* **1990**, *93*, 6987−7002.
(28) Purvis, G. D., III; Bartlett, R. J. A Full Coupled-Cluster Singles and Doubles Model: The Inclusion of Disconnected Triples. *J. Chem. Phys.* **1982**, *76*, 1910−1918.
(29) Raghavachari, K.; Trucks, G. W.; Pople, J. A.; Head-Gordon, M. A Fifth-order Perturbation Comparison of Electron Correlation Theories. *Chem. Phys. Lett.* **1989**, *157*, 479−483.
(30) Watts, J. D.; Gauss, J.; Bartlett, R. J. Coupled-Cluster Methods with Non-iterative Triple Excitations for Restricted Open-Shell Hartree-Fock and Other General Single-Determinant Reference Functions. Energies and Analytical Gradients. *J. Chem. Phys.* **1993**, *98*, 8718−8733.
(31) Bartlett, R. J.; Musial, M. Coupled-Cluster Theory in Quantum Chemistry. *Rev. Mod. Phys.* **2007**, *79*, 291−352.
(32) Werner, H.-J.; Knowles, P. J.; Manby, F. R.; Black, J. A.; Doll, K.; Heßelmann, A.; Kats, D.; Köhn, A.; Korona, T.; Kreplin, D. A.; et al. The Molpro Quantum Chemistry Package. *J. Chem. Phys.* **2020**, *152*, 144107-1−144107-24.
(33) Werner, H.-J.; Knowles, P. J.; G., Knizia, Manby, F. R.; Schütz, M.; Celani, P.; Györffy, W.; Kats, D.; Korona, T.; Lindh, R.; et al.. *MOLPRO, version 2019.2, A Package of Ab Initio Programs* (https://www.molpro.net) [Accessed January 1, 2021].
(34) Douglas, M.; Kroll, N. M. Quantum Electrodynamical Corrections to the Fine Structure of Helium. *Ann. Phys.* **1974**, *82*, 89−155.
(35) Jansen, G.; Hess, B. A. Revision of the Douglas-Kroll Transformation. *Phys. Rev. A* **1989**, *39*, 6016.

(36) Wolf, A.; Reiher, M.; Hess, B. A. The Generalized Douglas-Kroll Transformation. *J. Chem. Phys.* **2002**, *117*, 9215−9226.
(37) Kendall, R. A.; Dunning, T. H., Jr.; Harrison, R. J. Electron Affinities of the First-Row Atoms Revisited. Systematic Basis Sets and Wave Functions. *J. Chem. Phys.* **1992**, *96*, 6796−6806.
(38) De Jong, W. A.; Harrison, R. J.; Dixon, D. A. Parallel Douglas−Kroll Energy and Gradients in NWChem: Estimating Scalar Relativistic Effects Using Douglas−Kroll Contracted Basis Sets. *J. Chem. Phys.* **2001**, *114*, 48−53.
(39) Peterson, K. A. Correlation Consistent Basis Sets for Actinides. I. The Th and U Atoms. *J. Chem. Phys.* **2015**, *142*, No. 074105.
(40) Peterson, K. A.; Woon, D. E.; Dunning, T. H., Jr. Benchmark Calculations with Correlated Molecular Wave Function. IV. The Classical Barrier Height of the $H+H_2 \rightarrow H_2+H$ Reaction. *J. Chem. Phys.* **1994**, *100*, 7410−7415.
(41) Deegan, M. J. O.; Knowles, P. J. Perturbative Corrections to Account for Triple Excitations in Closed and Open Shell Coupled Cluster Theories. *Chem. Phys. Lett.* **1994**, *227*, 321−326.
(42) Rittby, M.; Bartlett, R. J. An Open-Shell Spin-Restricted Coupled Cluster Method: Application to Ionization Potentials in N_2. *J. Phys. Chem.* **1988**, *92*, 3033−3036.
(43) Knowles, P. J.; Hampel, C.; Werner, H.-J. Coupled Cluster Theory for High Spin, Open Shell Reference Wave Functions. *J. Chem. Phys.* **1993**, *99*, 5219−5228.
(44) Roos, B. O.; Taylor, P. R.; Siegbahn, P. E. M. A Complete Active Space SCF Method (CASSCF) Using a Density-matrix Formulated Super-CI Approach. *Chem. Phys.* **1980**, *48*, 157−173.
(45) Siegbahn, P. E. M.; Almlöf, J.; Heiberg, A.; Roos, B. O. The Complete Active Space SCF (CASSCF) Method in a Newton-Raphson Formulation with Application to the HNO Molecule. *J. Chem. Phys.* **1981**, *74*, 2384−2396.
(46) Andersson, K.; Malmqvist, P. A.; Roos, B. O.; Sadlej, A. J.; Wolinski, K. Second-Order Perturbation Theory with a CASSCF Reference Function. *J. Phys. Chem.* **1990**, *94*, 5483−5488.
(47) Andersson, K.; Malmqvist, P. A.; Roos, B. O. Second-Order Perturbation Theory with a Complete Active Space Self-Consistent Field Reference Function. *J. Chem. Phys.* **1992**, *96*, 1218−1226.
(48) Dunning, T. H., Jr. Gaussian Basis Set for Use in Correlated Molecular Calculations. I. The Atoms Boron Through Neon and Hydrogen. *J. Chem. Phys.* **1989**, *90*, 1007−1023.
(49) Ghigo, G.; Roos, B. O.; Malmqvist, P.-A. A Modified Definition of the Zeroth-Order Hamiltonian in Multiconfigurational Perturbation Theory (CASPT2) *Chem. Phys. Lett.* **2004**, *396*, 142−149.
(50) Berning, A.; Schweizer, M.; Werner, H.-J.; Knowles, P. J.; Palmieri, P. Spin-orbit Matrix Elements for Internally Contracted Multireference Configuration Interaction Wavefunctions. *Mol. Phys.* **2000**, *98*, 1823−1833.
(51) Dixon, D. A.; Feller, D.; Peterson, K. A. A Practical Guide to Reliable First Principles Computational Thermochemistry Predictions Across the Periodic Table. In *Annual Reports in Computational Chemistry*, vol 8, Wheeler, R. A., Section Ed. Tschumper, G. S., Eds.; Elsevier: Amsterdam, 2012, Ch. 1, pp 1−28.
(52) Feller, D.; Peterson, K. A.; Dixon, D. A. Further Benchmarks of a Composite, Convergent, Statistically-Calibrated Coupled Cluster-Based Approach for Thermochemical and Spectroscopic Studies. *Mol. Phys.* **2012**, *110*, 2381−2399.
(53) Peterson, K. A.; Feller, D.; Dixon, D. A. Chemical Accuracy in Ab Initio Thermochemistry and Spectroscopy: Current Strategies and Future Challenges. *Theor. Chem. Acc.* **2012**, *131*, 1079-1−1079-20.
(54) Feller, D.; Peterson, K. A.; Dixon, D. A. The Impact of Larger Basis Sets and Explicitly Correlated Coupled Cluster Theory on the Feller-Peterson-Dixon Composite Method. In *Annual Reports in Computational Chemistry*, Vol. *12*, Dixon, D. A., Ed.; Elsevier: Amsterdam, 2016, pp 47−78.
(55) Dunham, J. L. The Energy Levels of a Rotating Vibrator. *Phys. Rev.* **1932**, *41*, 721−731.
(56) Dyall, K. G. An Exact Separation of the Spin-Free and Spin-Dependent Terms of the Dirac-Coulomb-Breit Hamiltonian. *J. Chem. Phys.* **1994**, *100*, 2118−2127.
(57) Gomes, A. S. P.; Saue, T.; Visscher, L.; Jensen, H. J. A.; Bast, R. *DIRAC, a Relativistic Ab Initio Electronic Structure Program, Release DIRAC19*, 2019, (available at DOI: 10.5281/zenodo.3572669, see also http://www.diracprogram.org). Accessed April 25, 2022.
(58) Kállay, M.; Nagy, P. R.; Mester, D.; Gyevi-Nagy, L.; Csóka, J.; Szabó, P. B.; Rolik, Z.; Samu, G.; Csontos, J.; Hégely, B.; et al. *MRCC, A Quantum Chemical Program Suite*; Budapest University of Technology and Economics: Budapest. www.mrcc.hu. (Accessed May 1, 2022).
(59) Kállay, M.; Nagy, P. R.; Mester, D.; Rolik, Z.; Samu, G.; Csontos, J.; Csóka, J.; Szabó, P. B.; Gyevi-Nagy, L.; Hégely, B.; et al. The MRCC Program System: Accurate Quantum Chemistry from Water to Proteins. *J. Chem. Phys.* **2020**, *152*, No. 074107.
(60) Watts, J. D.; Bartlett, R. J. The Coupled-Cluster Single, Double, and Triple Excitation Model for Open-Shell Single Reference Functions. *J. Chem. Phys.* **1990**, *93*, 6104−6105.
(61) Noga, J.; Bartlett, R. J. The Full CCSDT Model for Molecular Electronic Structure. *J. Chem. Phys.* **1987**, *86*, 7041−7050.
(62) Kucharski, S. A.; Bartlett, R. J. Noniterative Energy Corrections through Fifth-Order to the Coupled Cluster Singles and Doubles Method. *J. Chem. Phys.* **1998**, *108*, 5243−5254.
(63) Reed, A. E.; Curtiss, L. A.; Weinhold, F. Intermolecular Interactions from a Natural Bond Orbital, Donor-Acceptor Viewpoint. *Chem. Rev.* **1988**, *88*, 899−926.
(64) Weinhold, F.; Landis, C. R. *Valency and Bonding: A Natural Bond Orbital Donor-Acceptor Perspective*; University Press: Cambridge, U.K., 2005.
(65) Glendening, E. D.; Landis, C. R.; Weinhold, F. NBO 7.0: New Vistas in Localized and Delocalized Chemical Bonding Theory. *J. Comput. Chem.* **2019**, *40*, 2234−2241.
(66) Glendening, E. D.; Badenhoop, J. K.; Reed, A. E.; Carpenter, J. E.; Bohmann, J. A.; Morales, C. M.; Karafiloglou, P.; Landis, C. R.; Weinhold, F. *Natural Bond Order 7.0, Theoretical Chemistry Institute*; University of Wisconsin: Madison, WI, 2018.
(67) Tang, R.; Si, R.; Fei, Z.; Fu, X.; Brage, T.; Liu, H.; Chen, C.; Ning, C. Candidate for Laser Cooling of a Negative Ion: High-Resolution Photoelectron Imaging of Th^-. *Phys. Rev. Lett.* **2019**, *123*, No. 203002.
(68) Zhu, Z.; Marshall, M.; Harris, R. M.; Bowen, K. H.; Vasiliu, M.; Dixon, D. A. The Th_2O^-, Th_2Au^- and $Th_2AuO_{1,2}^-$ Anions: Photoelectron Spectroscopic and Computational Characterization of Energetics and Bonding. *J. Phys. Chem. A* **2021**, *125*, 258−271.
(69) Curtiss, L. A.; Raghavachari, K.; Redfern, P. C.; Pople, J. A. Assessment of Gaussian-2 and Density Functional Theories for the Computation of Enthalpies of Formation. *J. Chem. Phys.* **1997**, *106*, 1063−1079.
(70) Fang, Z.; Lee, Z.; Peterson, K. A.; Dixon, D. A Use of Improved Orbitals for CCSD(T) Calculations for Predicting Heats of Formation of Group IV and Group VI Metal Oxide Monomers and Dimers and UCl_6. *J. Chem. Theory Comput.* **2016**, *12*, 3583−3592.
(71) Guillaumont, R.; Fanghånel, T.; Neck, V.; Fuger, J.; Palmer, D. A.; Grenthe, I.; Rand, M. H. *Chemical Thermodynamics 5: Update on the Chemical Thermodynamics of Uranium, , Neptunium, Plutonium, Americium and Technetium*; Elsevier: Amsterdam, 2003.
(72) Wagman, D. D.; Evans, W. H.; Parker, V. B.; Schumm, R. H.; Halow, I.; Bailey, S. M.; Churney, K. L.; Nuttall, R. L. The NBS Tables of Chemical Thermodynamic Properties. Selected Values for inorganic and C_1 and C_2 Organic Substances in SI units. *J. Phys. Chem. Ref. Data* **1982**, *11*, 2.
(73) Craciun, R.; Picone, D.; Long, R. T.; Li, S.; Dixon, D. A.; Peterson, K. A.; Christe, K. O. Third Row Transition Metal Hexafluorides, Extraordinary Oxidizers and Lewis Acids: Electron Affinities, Fluoride Affinities, and Heats of Formation of WF_6, ReF_6, OsF_6, IrF_6, PtF_6, and AuF_6. *Inorg. Chem.* **2010**, *49*, 1056−1070.
(74) Ruscic, B.; Pinzon, R. E.; Morton, M. L.; von Laszewski, G.; Bittner, S.; Nijsure, S. G.; Amin, K. A.; Minkoff, M.; Wagner, A. F. Introduction to Active Thermochemical Tables: Several "Key" Enthalpies of Formation Revisited. *J. Phys. Chem. A* **2004**, *108*, 9979−9997.

(75) Changala, P. B.; Nguyen, T. L.; Baraban, J. H.; Ellison, G. B.; Stanton, J. F.; Bross, D. H.; Ruscic, B. Active Thermochemical Tables: The Adiabatic Ionization Energy of Hydrogen Peroxide. *J. Phys. Chem. A* **2017**, *121*, 8799−8806.
(76) https://atct.anl.gov/Thermochemical%20Data/version%201.122g/index.php (accessed January 18, 2021).
(77) Konigs, R. J. M.; Morss, L. R.; Fuger, J. *Thermodynamic Properties of Actinides and Actinide Compounds in The Chemistry of the Actinide and Transactinide Elements*, 3rd Ed.; Morss, L. R., Edelstein, N. M., Fuger, J., Eds.; Springer: Dordrecht, 2006; Chapter 19, Vol. *4*, pp 2113−2224
(78) Craciun, R.; Long, R. T.; Dixon, D. A.; Christe, K. O. Electron Affinities, Fluoride Affinities, and Heats of Formation of the Second Row Transition Metal Hexafluorides: MF_6 (M = Mo, Tc, Ru, Rh, Pd, Ag). *J. Phys. Chem. A* **2010**, *114*, 7571−7582.
(79) Thanthiriwatte, K. S.; Vasiliu, M.; Battey, S. R.; Lu, Q.; Peterson, K. A.; Andrews, L.; Dixon, D. A. Gas Phase Properties of MX_2 and MX_4 (X=F, Cl) for M = Group 4, Group 14, Ce, and Th. *J. Phys. Chem. A* **2015**, *119*, 5790−5803.

Recommended by ACS

Electron Binding Energy Spectra of Al_nPt^- Clusters—A Combined Experimental and Computational Study
Paulo H. Acioli, Julius Jellinek, *et al.*
JUNE 24, 2022
THE JOURNAL OF PHYSICAL CHEMISTRY A
READ

Probing the Halide Effect in the δ-Bond with One- and Two-Photon Spectroscopy
Jack C. Boettcher, Daniel G. Nocera, *et al.*
JULY 25, 2022
THE JOURNAL OF PHYSICAL CHEMISTRY LETTERS
READ

Electronic Structure of RhO^{2+}, Its Ammoniated Complexes $(NH_3)_{1-5}RhO^{2+}$, and Mechanistic Exploration of CH_4 Activation by Them
Shahriar N. Khan and Evangelos Miliordos
OCTOBER 12, 2021
INORGANIC CHEMISTRY
READ

Quantum Inelastic Scattering of $ArHAr^+$, $HeHHe^+$, and $NeHNe^+$ with He on New Potential Energy Surfaces
Otoniel Denis-Alpizar, Ricardo Pino-Rios, *et al.*
JULY 05, 2022
ACS EARTH AND SPACE CHEMISTRY
READ

Get More Suggestions >

https://doi.org/10.1021/acs.jpca.2c03115
J. Phys. Chem. A 2022, 126, 4432−4443